Available online at www.sciencedirect.com
SCIENCE DIRECT®
Acta Materialia 53 (2005) 4281–4292
Acta MATERIALIA
www.actamat-journals.com

The crustacean exoskeleton as an example of a structurally and mechanically graded biological nanocomposite material

D. Raabe *, C. Sachs, P. Romano

Max-Planck-Institut für Eisenforschung, Max-Planck-Str. 1, 40237 Düsseldorf, Germany

Received 11 April 2005; received in revised form 20 May 2005; accepted 20 May 2005
Available online 14 July 2005

Abstract

This is an experimental study on the mechanical and structural gradients through the cuticle of *Homarus americanus* (American lobster). The exocuticle (outer layer) is characterized by a very fine woven structure of the fibrous chitin–protein matrix ('twisted plywood' structure) and by a high stiffness (8.5–9.5 GPa). The hardness increases within the exocuticle between the surface region (130 MPa) and the region close to the interface to the endocuticle (270 MPa). In the endocuticle, which is characterized by a much coarser twisted plywood structure, both the stiffness (3–4.5 GPa) and hardness (30–55 MPa) are much smaller than in the exocuticle. The transition in mechanical properties and structure between the exocuticle and endocuticle is abrupt. The differences underline the important role of the internal structure of the twisted plywood structure and of the interface between the two cuticle layers for the overall mechanical behavior of the exoskeleton. The excellent mechanical stability of the interface (irrespective of the change in the mechanical properties) is attributed to the fact that the structural change of the twisted plywood pattern across the interface consists only of a change of the stacking density of the chitin–protein layers. The observed gradients in stiffness and hardness through the cuticle thickness are interpreted in terms of honeycomb mechanics of the twisted plywood structure. The possible role of gradients in protein cross-linking and in the mineral content is also discussed.

Keywords: Mineralized tissue; Indentation; Bouligand structure; Biological composite; Biomineralization

1. Introduction

The exoskeleton material of arthropods consists of mineralized fibrous chitin-based tissue [1,2]. The most characteristic feature of this biological nanocomposite material is its strictly hierarchical organization which reveals various structural levels [2–6]: at the molecular level is the polysaccharide chitin itself. Its antiparallel alignment forms α-chitin crystals [7–9]. The next structure level is the arrangement of 18–25 of such molecules in the form of narrow and long crystalline units, which are wrapped by proteins, forming nanofibrils of about 2–5 nm diameter and about 300 nm length [2–6]. The next step in the scale consists in the clustering of some of these nanofibrils into long chitin–protein fibers of about 50–300 nm diameter (Fig. 1).

These chitin–protein fibers form a planar woven and periodically branched network (chitin–protein layers). The spacing between the fibers is filled up with proteins and biominerals of microscopic and nanoscopic size [2,4,10–16]. The minerals are mostly in the form of crystalline $CaCO_3$, but amorphous particles may also occur depending on the species and molt cycle. The most characteristic level in the overall hierarchy, visible even in an optical microscope, is referred to as a twisted plywood

* Corresponding author. Tel.: +49 211 6792 278/340.
E-mail address: raabe@mpie.de (D. Raabe).

1359-6454/$30.00
doi:10.1016/j.actamat.2005.05.027

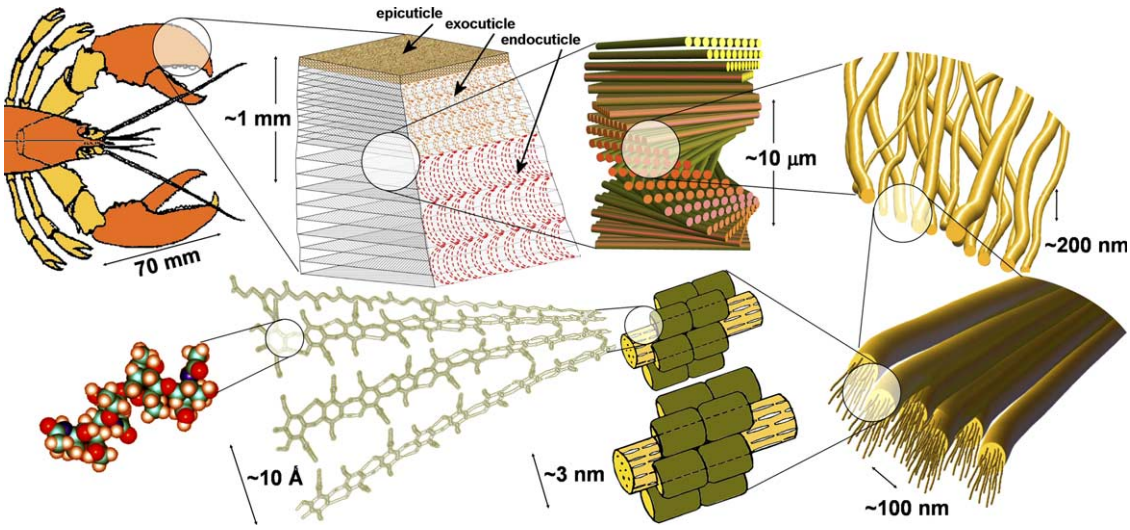

Fig. 1. Hierarchy of the main structural levels and microstructure elements of the exoskeleton material (referring to the exocuticle and endocuticle layers) of *H. americanus* (American lobster). The first structure level (Bouligand or respectively twisted plywood pattern) is presented as a cross section through the thickness of the cuticle.

or Bouligand pattern [17–20]. This structure is formed by the helicoidal stacking sequence of the fibrous chitin–protein layers (Fig. 1). The thickness of one such twisted plywood or Bouligand layer corresponds to a certain stacking density of planes which are gradually rotated about their normal axis, thereby creating complex structures which appear as mesoscale arches when cut in cross sections [17–20].

This study presents observations, which substantiate that this structural picture of the exoskeleton material of arthropods must be completed by an additional feature, namely, by the occurrence of a pronounced mesoscopical structural gradient of the twisted plywood pattern through the thickness of the exoskeleton material. Corresponding microindentation tests which were carried out through the cuticle thickness further suggest that the structure gradients observed play an important role for the micromechanical design strategy inherent to such materials.

The experiments are conducted on the cuticle of the lobster *Homarus americanus*. This animal is a large arthropod (joint-limb animal) which belongs to the class of the crustaceans and the order of the decapods [21,22]. Its cuticle consists, like that of most arthropods, of the three main layers, epicuticle, exocuticle, and endocuticle, which are secreted by a single layer of epidermis cells. The epicuticle (outer skin) is a very thin and waxy functional layer, which acts as a diffusion barrier to the surrounding. The exocuticle and endocuticle layers, which carry the mechanical loads, consist of a hard mineralized fibrous chitin–protein tissue as described above. The experimental results shown in this study stem from these two layers.

2. Experimental

2.1. Microscopy, sample preparation, and mechanical testing

The exoskeleton of the lobster *H. americanus* was analyzed by using microscopy and mechanical testing. The sample material consisted of dry specimens cut from the right cheliped (pincher claw). The microstructure was characterized by using transmission and reflection light optical microscopy (Leica DM 4000B) and scanning electron microscopy (CamScan 4). Samples for reflection light optical microscopy were prepared by polishing and gold coating. Samples for transmission light optical microscopy were cut to 5 µm thickness by using a rotary microtome (Leica RM 2165). Both types of specimens were prepared as cross sections. The samples for scanning electron microscopy were additionally prepared as gold-coated sections parallel to the surface. Mechanical testing was conducted via microindentation testing using a Fischerscope H100C hardness tester. This device was used for an indentation procedure during which the penetration depth was registered as a function of the applied load (load range: 1–1000 mN). The experimental error amounted to 0.2 µN for the load and about 0.5 nm for the indentation depth. In the current study the maximum load was 500 mN. The indenter was a Vickers pyramid with an angle of 136°. The deformation analysis was based on the assumption that unloading is fully reversible so that the indent mechanics can be approximated in terms of Hertzian contact theory.

2.2. On the meaning of elasticity and stiffness of biological matter at the microscopic scale

While the interpretation of hardness data determined by microindentation on biological samples follows similar principles to synthetic soft matter the meaning of terms such as elasticity or stiffness extracted from such experiments deserves a closer analysis.

When hierarchically structured materials are subjected to small mechanical loads one has to separate the intrinsic elastic modulus from the microstructural stiffness as two distinctly different types of linear mechanical response. The intrinsic elastic modulus is the linearized second derivative of the interatomic potential of the electronic bond between the atoms of the structure, which is probed by the indenter. It is, hence, an electronic property, which reflects the nature of the bond in an electronically homogeneous portion of matter. In homogenous bulk materials small scale hardness tests can, therefore, provide data for the electronic (intrinsic) elastic modulus when using Hertzian contact mechanics in conjunction with Hooke's law. For instance, the assumption of an elastically isotropic contact during indentation allows one to determine the reduced elastic modulus, E_r, from an unloading experiment. This term is defined as $E_r = \left[(1-v_a^2)/E_a + (1-v_b^2)/E_b\right]^{-1}$, where E_a, E_b, v_a, and v_b are the elastic moduli and Poisson's ratios of the indented material (subscript 'a' for the biological material) and of the indenter material (subscript 'b' for the indenter), respectively. For a combination of a rigid indenter and a comparatively soft specimen $E_b \gg E_a$ applies so that $E_r \approx E_a/(1-v_a^2)$. Of course, this approximation holds only for the isotropic case.

In contrast to such a situation which applies to most homogeneous materials, indentation experiments on heterogeneous and hierarchically structured nanocomposite samples such as encountered in the case of mineralized biological tissue (Fig. 1), provide data, which reflect the stiffness of the entire microstructure affected by the indent. This means that in such a situation indentation tests probe the microstructural stiffness. In contrast to the electronic elasticity, this property is an extrinsic material feature, which reflects an averaged linearized structural response of a *heterogeneous* portion of matter to an external mechanical load. This response may include the additive influence of a variety of possible elastic or pseudo-elastic effects depending on the microstructure and on the degree of heterogeneity of the material indented. Various mechanisms are conceivable which may add to the linear microstructural stiffness beyond the electronic elastic modulus in the case of biological samples, namely, microplasticity occurring in the various phases, structural deformation processes of the saccharide–protein network (honeycomb mechanics), interface delamination, or microscopic crack tip opening and closing effects.

The consideration that indents placed into biological materials average over various possible mechanisms (both in the linear and in the non-linear loading regime) is exploited in the present work for the investigation of lateral changes in the structural compliance through the thickness of the lobster exoskeleton. For this reason, the modulus data determined by microindentation in this study provide mainly structural rather than elastic information and we refer to them as reduced stiffness in the ensuing discussion. Owing to the complexity inherent in the various mechanisms delineated above one has, in principle, also to consider the time dependence of indentation forces. However, in order to avoid time effects in the current study all indents were conducted at the same loading rate with the same loading time.

3. Experimental results on through-thickness gradients of hardness and stiffness

Fig. 2 shows the lateral distribution of the hardness (Fig. 2(a)) and of the reduced stiffness (Fig. 2(b)) as determined by microindentation through the thickness of the dry claw cuticle of lobster *H. americanus*. Both the hardness and the reduced stiffness reveal pronounced gradients between the surface and the sample interior.

The course of the hardness through the cuticle thickness shows two main characteristics. First, it reveals a strong and abrupt change across the interface between the exocuticle and the endocuticle (Figs. 2(a) and 3). Second, the hardness reveals a gradual increase within the exocuticle between the epicuticle and the endocuticle layers. In the near-surface region below the epicuticle (100 μm depth) it assumes a value of about 130 MPa. The hardness then steadily increases by a factor of two up to a maximum of 270 MPa. This peak value occurs about 50 μm before the interface between the exocuticle and the endocuticle at 300 μm depth from the surface (Fig. 3). After a small drop from 270 to 240 MPa at 350 μm depth (close to the interface layer between exocuticle and endocuticle, Fig. 3) the hardness decreases to a much lower level, between 30 and 55 MPa, in the endocuticle. It is remarkable that this transition in hardness between the two main cuticle layers is so steep, amounting to nearly one order of magnitude across the interface.

The change in stiffness between the two layers is also large (Fig. 2(b)). Within the exocuticle, the reduced stiffness is characterized by a high and relatively constant level of 8.5–9.5 GPa. When entering the endocuticle layer the stiffness drops by more than a factor of two to a level of 3–4.5 GPa. This means that both the hardness and the stiffness show a strong discontinuity across the interface between the exocuticle and the endocuticle.

Fig. 3 reveals that the Bouligand layers are characterized in part by a wavy appearance and by a spatial

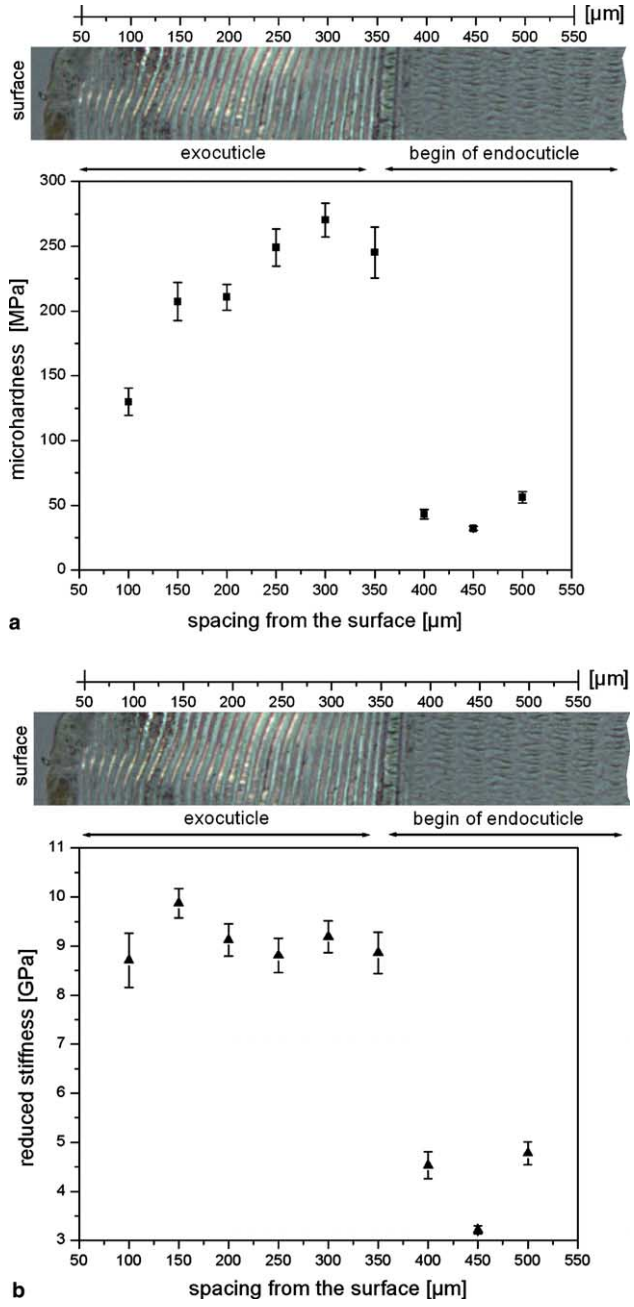

Fig. 2. The hardness and the reduced stiffness reveal a pronounced gradient through the thickness of the dry exoskeleton of lobster *H.americanus*. A strong discontinuity occurs at the interface between the exocuticle and the endocuticle. The data are shown together with a micrograph of a cross section through the thickness of the cuticle in order to document at which depth the data were taken (the complete micrograph is shown in Fig. 3).

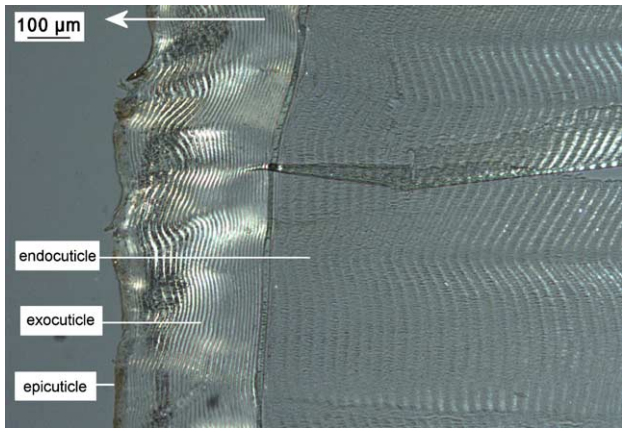

Fig. 3. Light optical micrograph of a cross section through the thickness of the claw of *H. americanus*. The area shows the range in which the indentation tests were carried out (the picture does not, however, exactly show the same portion of material where the indents were placed). The arrow points in the surface direction of the exoskeleton. The cuticle of lobster consists, like that of most arthropods, of the three main layers epicuticle, exocuticle, and endocuticle (Fig. 1). The epicuticle (outer skin) is a very thin and waxy layer, which acts as a diffusion barrier. The exocuticle and endocuticle layers are designed to resist mechanical loads. They consist of a hard fibrous chitin–protein tissue containing calcium carbonate minerals (mostly crystalline, sometimes amorphous). The two layers (exocuticle and endocuticle) reveal the well-known twisted plywood structure, which is characteristic of the arthropod cuticle.

variation of their thickness (which results from the stacking density of the chitin–protein planes). The structural variation in the thickness of these layers seems to be more pronounced in the exocuticle while in the endocuticle the layers appear more homogeneous. It is conceivable that these structural variations in the plywood-type pattern are due to some degree of lateral and kinetic heterogeneity during the synthesis of the chitin–protein planes and their stacking sequence after the molt.

4. Discussion

Since the pioneering work of Bouligand [17] and Giraud-Guille [18–20] it is known that the twisted plywood pattern, which is characteristic of the cuticle of arthropods, is formed by a certain stacking sequence of the chitin–protein layers. These flat structural units are planar woven and periodically branched arrays of chitin–protein fibers which in turn consist of bundles of protein-wrapped crystalline α-chitin nanofibrils (Fig. 1) [3,4,9].

The planes are arranged in the form of helicoidal stacks which are gradually rotated about their normal (zone axis), i.e., each plane is misoriented with respect to the preceding one (Fig. 4). It should be noted that the details of the orientational order of the stacking sequence might vary. Certain preferred variants of rotations (with the same zone axis) have been reported by Weiner et al. [23–25] and by Raabe et al. [26]. Also, the chitin–protein planes do not exactly consist of sets of perfectly aligned parallel fibers as schematically indi-

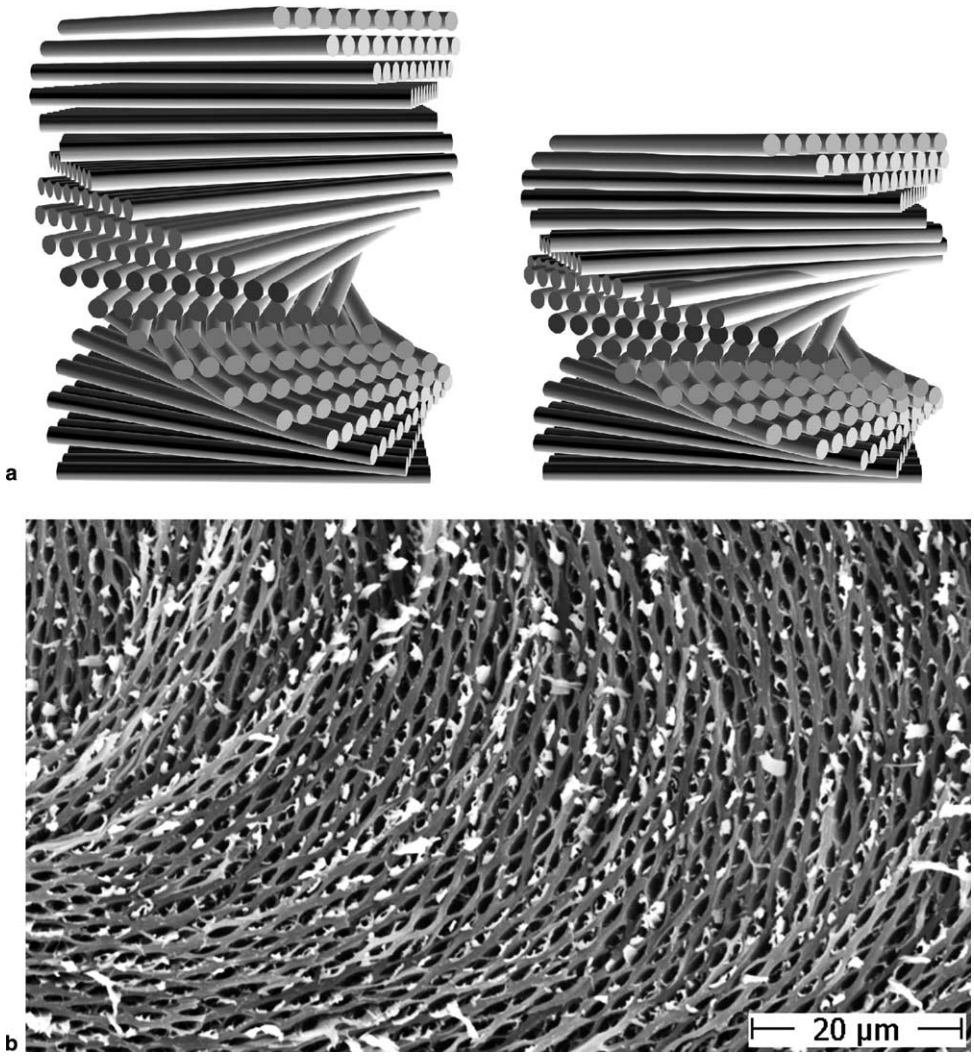

Fig. 4. (a) Simplified schematical presentation of two possible versions of Bouligand patterns. The two examples are characterized by a different stacking density of the constituent chitin–protein planes such as encountered in the endocuticle (low stacking density) and in the exocuticle (high stacking density). The details of the orientational order of the stacking sequence may vary. Certain preferred variants of rotations (with the same zone axis) have been reported earlier by Weiner et al. [23–25] and recently by Raabe et al. [26]. It should be noted that the chitin–protein layers do not really consist of sets of perfectly parallel fibers as indicated in the drawings, but they form flat honeycomb-type arrays in the lobster cuticle such as those visible in the SEM in-plane view shown in (b).

cated in Fig. 4 for better transparency, but they tend to form flat honeycomb-type arrays in the lobster cuticle.

The thickness of the twisted plywood or respectively Bouligand layers corresponds to the stacking height of the chitin–protein planes that is required for an accumulated rotation of 180° about their normal direction (Fig. 1). This means that small-scale patterning is a feature inherent to such twisted plywood-type structures and that their thickness or characteristic wavelength (when cut oblique) is a function of the stacking density of the constituent chitin–protein planes (Figs. 4 and 5).

When considering this constructional principle the most obvious correlation between the through-thickness microstructure and the mechanical gradients observed (Fig. 2) is the difference in the structure of the twisted plywood pattern between exocuticle and endocuticle (Fig. 3). This is also documented in Fig. 5, which presents a set of through-thickness micrographs showing in particular the interface region between the exocuticle and the endocuticle. The pictures substantiate that a pronounced change in the twisted plywood structure occurs across the interface between the exocuticle and the endocuticle where the mechanical discontinuity occurs. The micrographs in Figs. 3 and 5 as well as the quantitative data in Fig. 6 show that the exocuticle is characterized by a much finer stacking density of the fibrous chitin–protein planes than the endocuticle. The analysis of 18 samples (Fig. 6(a)) shows that the exocuticle is characterized by a very fine woven structure of the chitin–protein matrix with an average stacking height (thickness) of the twisted plywood layers of 9.4 μm. The endocuticle is characterized by a much coarser matrix structure. The average thickness of the

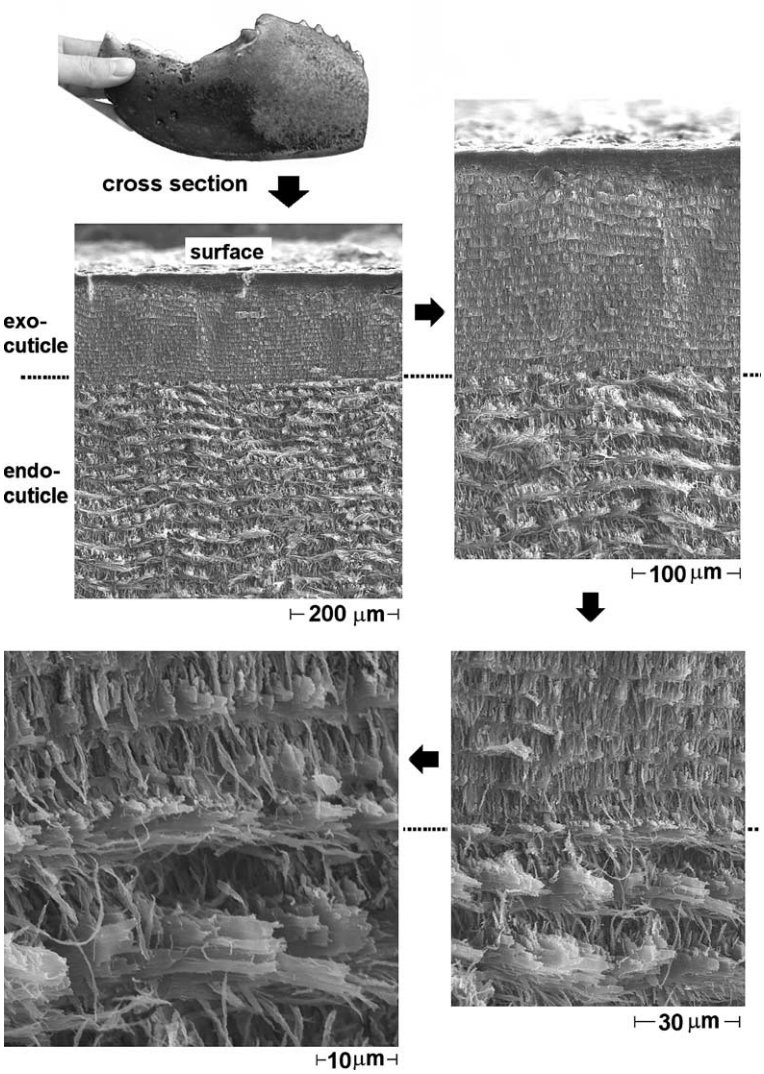

Fig. 5. A series of through-thickness SEM micrographs, which show in particular the interface region between the exocuticle and the endocuticle in increasing resolution. The images were taken on fractured surfaces in order to observe the true stacking density and avoid smear-out type damage from the microtome or from a polishing procedure. The micrographs reveal that a pronounced change in the twisted plywood structure exists across the interface between the exocuticle and the endocuticle. The location of the mechanical discontinuity (Fig. 2) occurs at the same position as the change in the stacking density of the twisted plywood layers, i.e., the exocuticle has a much finer structure (stacking density of the fibrous chitin–protein planes) than the endocuticle.

twisted plywood planes in this layer amounts to 35.1 μm (Fig. 6(b)). It must be emphasized that within both layers, considerable deviations from the average values can occur locally as is visible qualitatively in Fig. 3 and which is quantitatively documented in Fig. 6. These variations amount to a range of 7–11.5 μm in the exocuticle and 19–45 μm in the endocuticle.

This means that the stacking density of the chitin–protein planes (thickness of one Bouligand layer) changes on average by a factor of about 3.7 across the interface between the exocuticle and the endocuticle. This ratio does not match the observed change in the reduced stiffness between the two layers (factor of 2.4: 8.5–9.5 GPa in the exocuticle versus 3–4.5 GPa in the endocuticle, Fig. 2(b)), at least not one-to-one.

It is important in this context that the fibers which constitute the chitin–protein planes neither form randomly packed nor highly parallel arrays but reveal a strong resemblance to a honeycomb structure. Figs. 4(b) and 7 show such planes when viewed from a slightly inclined surface normal direction, i.e., roughly perpendicular to the direction of the indent. The open structure visible in those micrographs has been obtained by a pull-out deformation experiment in which the second chitin–protein honeycomb layer which usually interpenetrates the one depicted (Fig. 5) has been mechanically removed.

The (incomplete) microstructure shown in Figs. 4(b) and 7 suggests that it is pertinent in this context to consider the micromechanics associated with honeycombs when aiming at an interpretation of the stiffness observed

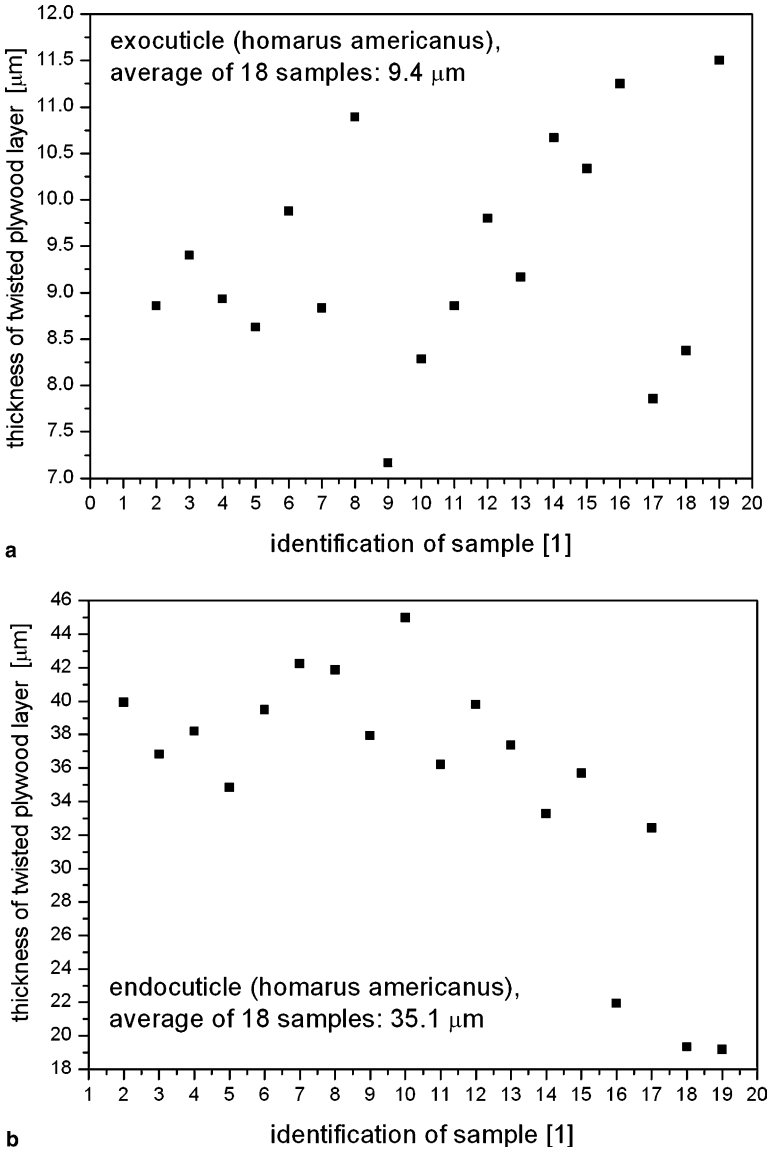

Fig. 6. Statistics of the thickness of the twisted plywood layers in the exocuticle and in the endocuticle.

[27–31]. Such analysis must of course remain on a somewhat qualitative level at this stage but it might help to identify the degree of correlation between the observed mesostructure (Figs. 5 and 7) and the linear compliance of the cuticle (Fig. 2(b)).

Let us assume for the moment that the local stiffness of the exoskeleton material is chiefly determined by the structural compliance of the twisted plywood pattern and that this compliance essentially arises from the stiffness of its constituent chitin–protein honeycombs (Figs. 7 and 8). Further, we make the assumption that a structural principle of similitude applies. This means that the segment length, which characterizes the density of the honeycomb structure (Fig. 8) in each of the two cuticle layers (endo- and exocuticle) is assumed to follow the scaling observed for the stacking density of the twisted plywood pattern as presented in Fig. 6. This assumption implies that the ratio between the segment wall thickness, t, and the segment length, ℓ, changes between the two layers. This assumption is plausible since the segment thickness is not a mesoscopic quantity such as the length of the honeycomb segments but it is primarily determined by the agglomeration of the chitin–protein fibrils (Fig. 1).

When loaded parallel to the plane normal as in the present case of indentation (mode of largest stiffness) the total stiffness modulus of one single honeycomb layer can be described in a linear fashion in the form of a hyperbolic function of the microstructure, i.e., $E_{x_3}/E_s \approx t/\ell$, where E_{x_3} is the stiffness of the honeycomb along the x_3 direction (out-of-plane direction, plane normal, loading direction), E_s the bulk stiffness, t the segment thickness, and ℓ the segment length of the honeycomb structure (Figs. 8(a) and 9) [27,28]. For this

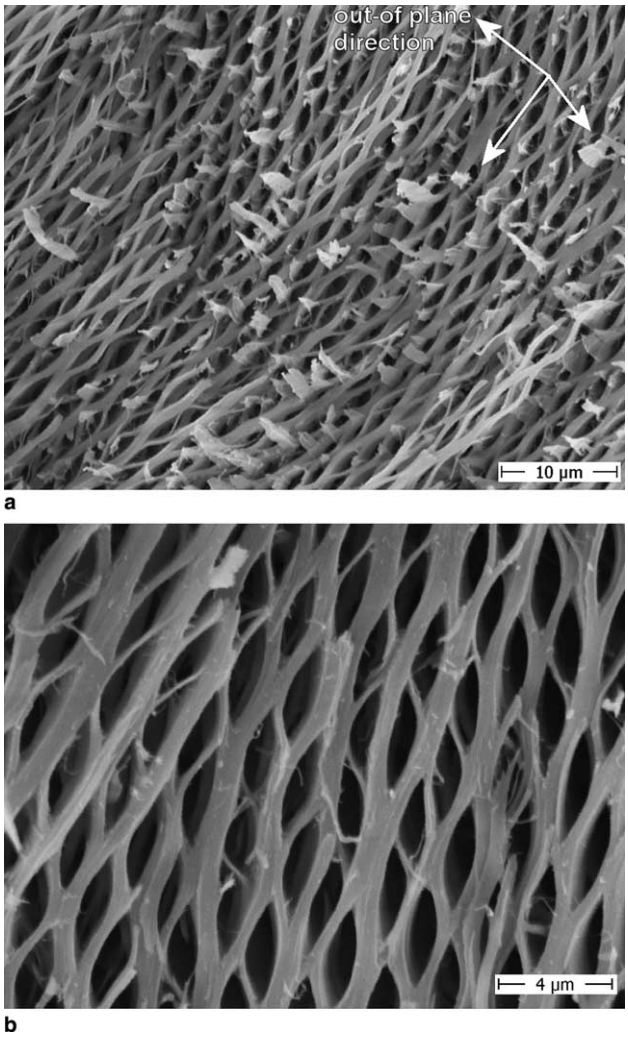

Fig. 7. Micrographs taken by scanning electron microscopy. They show the honeycomb topology of the woven chitin–protein layers.

case the stiffness changes inversely proportional to the segment length and linearly (one-to-one) with the ratio between wall thickness and segment length. For an in-plane loading mode (E_{x_1}, E_{x_2}) the stiffness of a perfectly homogeneous honeycomb follows a third-order polynomial, namely, $E_{x_1}/E_s = E_{x_2}/E_s \approx (t/\ell)^3$ where the x_1 and x_2 directions are the two principal vectors within the plane. The in-plane mode is the softest possible loading mode for a honeycomb structure [27,28].

An alternative approximation of the observed structure consists in speculating that the overall stiffness is comprised of the joint resistance of two interpenetrating sets of honeycomb layers as visible in Figs. 5 and 7(a) and as schematically indicated in Fig. 8(b). We refer to this loading situation as the mixed mode. Of course, more detailed experiments must be conducted to exactly determine the true structure and volume fraction of the second layer which interpenetrates the main honeycomb layer visible in Fig. 7.

An approximate estimate of the relationship between structure and stiffness can in such a case be made by an equal partition of in-plane and out-of plane contributions. A linear ansatz for this mixed mode, therefore, yields $E_{mix}/E_s = 1/2(t/\ell) + 1/2(t/\ell)^3$.

The introduction of such a simple rule of mixture is motivated by Figs. 5 and 7(a) as well as by results presented in [26]. These data reveal that the normals of the two sets of honeycomb structures have a mutual misorientation close to 90°, i.e., the layers are nearly perpendicular to each other. This observation is translated into the assumption of a parallel arrangement of the two honeycomb orientations where 50% of the volume is loaded in the in-plane mode and 50% in the out-of-plane mode. Since the thickness-to-length ratio is quite small for the honeycomb structure encountered, the third-order contribution of the in-plane mode becomes insignificant. This means that the mixed mode reflects essentially that the stiffness observed originates from only 50% of the loaded honeycomb volume. Of course, a more detailed model would have to account for the dependence of this rule of mixture on the direction of the load imposed.

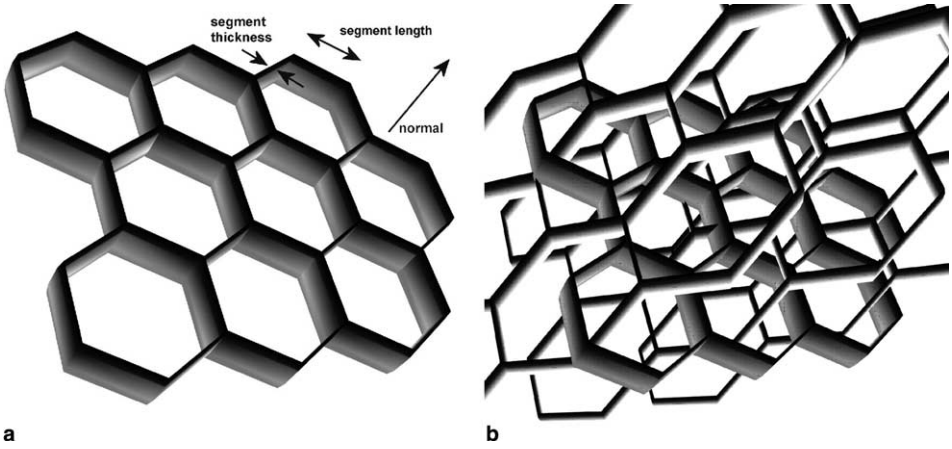

Fig. 8. Schematic sketch of the honeycomb network: (a) one chitin–protein network plane (compare to Fig. 7(b)); (b) two sets of interpenetrating chitin–protein planes (cf. Figs. 5 and 7(a)). Figs. 5 and 7(a), as well as corresponding data presented in [26], suggest that the normals of the two sets of honeycomb structures have a mutual misorientation close to 90°.

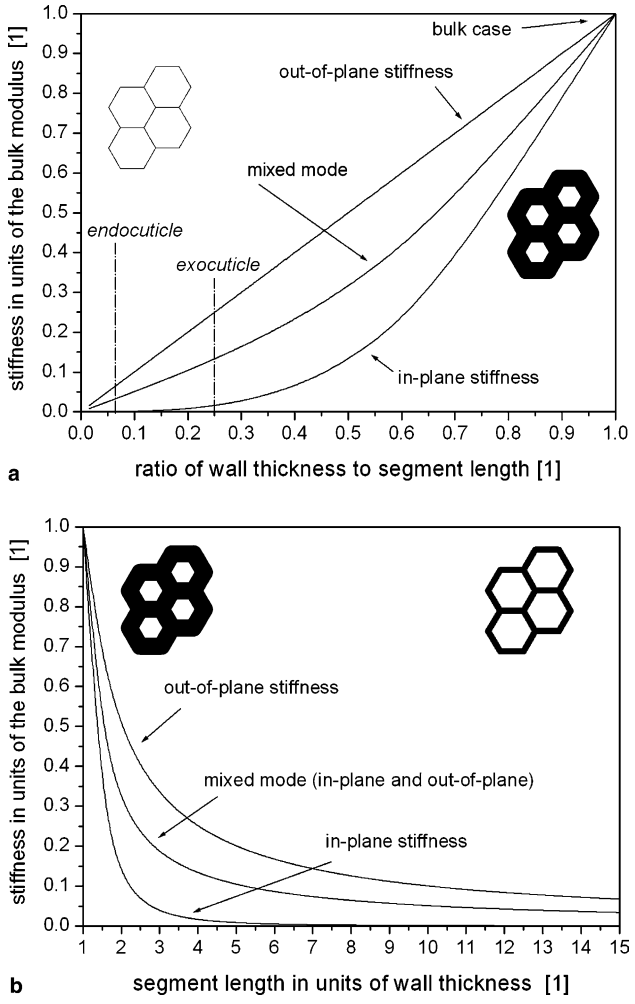

Fig. 9. Analytical solutions for three topological cases of the reduced structural stiffness of a chitin–protein honeycomb (out-of plane stiffness, in-plane stiffness, mixed mode). The analytical solutions for the out-of plane and for the in-plane stiffness are taken from the work of Gibson and Ashby [27,28].

However, for the present discussion the 50:50 mix seems appropriate owing to the strong alignment of the honeycombs either parallel or perpendicular to the surface normal which corresponds to the loading direction (Fig. 5). The solution for the mixed mode case is – in terms of the overall stiffness – located between the hard out-of-plane and the soft in-plane mode. The three different solutions (out-of plane stiffness, in-plane stiffness, mixed mode) are shown in Fig. 9.

Fig. 9(a) indicates, together with the three solutions, typical numbers for the ratio between wall thickness and honeycomb segment length for the cuticle investigated in this study (vertical lines marked by the terms exocuticle and endocuticle). The stiffest solution is the out-of-plane approach. It reproduces a linear one-to-one structure–stiffness relationship (for loads parallel to the plane normal of one orientational variant of the honeycomb substructure). This means that the increase in stiffness which could have been expected for the observed changes in the twisted plywood structure across the interface between the exocuticle and the endocuticle (Fig. 6) would be one-to-one. The experimental stiffness data, however, show a drop by a factor of only 2.4 (Fig. 2(b)). This means that the linear out-of-plane solution seems to be somewhat too stiff. The mixed-mode solution predicts a smaller drop in stiffness upon the same change in structure which seems to be more likely in view of the complexity of the interpenetrating honeycombs and the stiffness data observed.

Hence, the qualitative estimate presented in Fig. 9 suggests that the drop in stiffness between the exocuticle and the endocuticle cannot be attributed to the resistance of one representative honeycomb layer loaded along the out-of-plane direction alone but to the joint stiffness of a more complex structure which also experiences in-plane loading contributions. However, the calculations do show that the stiffness of the entire twisted plywood structure seems to depend indeed in a rather simple fashion on the joint mechanical resistance of the stacked fibrous chitin–protein honeycombs. Other effects which might in principle also show a linear response at least under the influence of small loads, such as microplasticity or microcrack effects within the honeycomb structure, seem to play a less relevant role in the overall compliance observed.

One plausibility check of the honeycomb-based approximation of the stiffness observed lies in comparing the absolute stiffness values shown in Fig. 2 with literature data of the bulk modulus of chitin fibrils in conjunction with the honeycomb equations given above. Nishino et al. [32] have published data for the elastic modulus of the crystalline regions of chitin and chitosan which they obtained by X-ray diffraction. They reported that the elastic moduli of the (dry) crystalline regions of α-chitin and chitosan in the direction parallel to the chain axis amounted to 41 GPa for α-chitin at 20 °C. Using this number in the honeycomb equation for the mixed mode yields as absolute values for the structure stiffness 5.45 GPa for the exocuticle and 1.23 GPa for the endocuticle. These values are below those observed in the experiment (Fig. 2). Ker [33] reported a value of 20 GPa measured parallel to the chitin orientation in the tibial flexor apodeme of the locust. This bulk value translates to a structure stiffness of 2.66 GPa for the exocuticle and 0.6 GPa for the endocuticle. These values are even smaller than those derived with the data of Nishino et al. [32]. Yamaguchi et al. [34] have reported even smaller numbers for the modulus of chitin, namely, 8.47 GPa. However, since this value was obtained from tensile tests it is likely that it represents the net structure modulus of the entire microstructure rather than the elastic modulus of one single chitin fiber (see comments on the difference between these two types of quantities in Section 2.2).

In this context one should also mention that there have been two reports of explicit values for the stiffness of the chitin lamella (and not for a homogenized tensile specimen). Xu et al. [35] reported values for the Young's modulus for single chitin fibers of the order of 100–200 GPa. This large value is in line with a report of Vincent who mentioned [4] that the modulus of chitin lamellae might be as large as 130 GPa or even higher. The resulting honeycomb stiffness would amount to 17.3 GPa in the exocuticle and 3.9 GPa in the endocuticle.

Of course there is no reason to expect a perfect match between the simple honeycomb model outlined above and the experimental stiffness data. Rather, one should also extend the discussion towards effects other than those arising from the chitin–protein network. On the one hand, it is quite obvious that the profound structural changes across the interface between the exocuticle and the endocuticle as clearly documented in this study (Figs. 3, 4(b), and 5–7) are closely related to the observed gradients in the mechanical properties (Fig. 2). On the other hand, the deviation between the experimental values depicted in Fig. 2(b) and those derived by the help of literature data for the chitin in conjunction with the honeycomb model are not too surprising. This is due to the fact that up to this point we have anticipated that the stiffness observed is only due to the structural stiffness of the chitin–protein honeycombs, i.e., we neglected so far the influence of the minerals and of the protein matrix on the overall stiffness response.

In their papers on the arthropod cuticle Vincent [4,36,37] and Vincent and Wegst [3] have discussed the contributions of the different phases occurring in such plywood-type composites, namely, that of the fibrous crystalline chitin phase, of the stiffened protein matrix, and of the calcium minerals. Similar discussions can be found in [38–43]. Depending to the actual structures encountered they state that the stiffness of the cuticle can range from tens of GPa down to 1 kPa which emphasizes the relevance of contributions beyond those of the chitin–protein honeycomb lattice alone. In particular, the contribution of the secondary-bond cross-linking of the non-crystalline protein matrix seems to be important in that context [4,44].

As a third contribution to the overall cuticle stiffness is that of the mineral phase: Fratzl et al. [45–48] discussed the role of minerals for the stiffness of biological composites (using mostly the example of bone) in terms of a model where the microstructure consists of staggered mineral bricks such as the mineral platelet arrangement in collagen fibrils. In this approach, the mineral platelets carry their relative portion of the elastic load whereas the protein matrix transfers the load between mineral crystals via shear. The path of load transfer in such a model composite is in the form of a serial spring system consisting of mineral elements which are loaded in tension and protein elements which are loaded in shear. The model assumes a rather large aspect ratio of the mineral platelets such as observed in biological matter with large volume portions of mineral phase.

As a further aspect it must be considered that in the discussion above the various micromechanical assumptions are all based on the absence of water. This is in accordance with the experiments (Fig. 2) which were conducted on dry specimens. It is clear though that a more general discussion of the mechanical properties of biological matter beyond the gradient data presented in this work must consider the water content [4,49–52].

Thanks to its linear nature, the discussion of the cuticle stiffness and corresponding through-thickness gradients (Fig. 2(b)) can be conducted on the basis of a variety of earlier experimental data, detailed structural information, and some elementary models as shown above. An interpretation of the observed hardness data (Fig. 2(a)) though has to depart from less solid ground due to its inherent non-linearity. The deviation from linearity in the mechanical response of mineralized tissue beyond elasticity has three main sources. The first one is the individual non-linear elastic–plastic response of each of the three main different mechanical phases (minerals, protein matrix, chitin honeycombs). The second one is the nature of the mechanical interaction among the different phases when stressed beyond the linear (elastic) stiffness limit including interface mechanics. The third one is the mechanics associated with ubiquitous non-catastrophic micro-failure mechanisms.

Following the work of Vincent et al. [3–5,37], Currey [38,39] and others [40–43] as well as our own previous observations [26,53] and our current work, it may be stated that plastic yielding of the protein matrix, multiple shear and delamination effects along the different types of heterophase interfaces, microcracking particularly in the minerals and in the chitin–protein network (Fig. 5), and the non-linear and non-reversible yielding of the honeycomb structures mainly seem to contribute to the strength and hardness characteristics observed for the lobster cuticle. Owing to classical micromechanical models designed for understanding synthetic composites it is likely that two aspects play a key role in the absolute values of the hardness observed. These are first, the amount of the hard phase embedded in the (softer) matrix (the mineral phase in the current case) and second, the microstructural scaling which manifests itself in the occurrence of a very high density of homophase and heterophase interfaces. The first aspect (content of hard particles) cannot be quantitatively linked to the hardness gradients observed in this work because we do not yet have robust experimental data on possible gradients of the mineral content and distribution across the thickness of the cuticle. However, in view of the data

and micrographs shown in Figs. 2(a), 3, 5, and 6, the second aspect (interface density, structure of the twisted plywood pattern) seems to be of special relevance for the observed gradients in the hardness. We found that it increases within the exocuticle (which has a very fine plywood structure) between the surface and the interface to the endocuticle. The endocuticle (which has a much coarser twisted plywood structure) reveals a hardness level much below that in the exocuticle. The difference in hardness between the two layers amounts to nearly one order of magnitude, i.e., the drop is much more pronounced than that of the linear portion of the stiffness. Since the transition between the two layers is abrupt, one may conclude that the stacking density of the mutually misoriented chitin–protein planes must play a dominant role in the hardness.

In this context one should mention that in all mechanical experiments presented in this study the interface between the exocuticle and the endocuticle (Fig. 5) revealed a remarkable mechanical stability irrespective of the change in the mechanical properties. This property could be due to the fact that the structure change between the two layers occurs simply in the form of a change in the stacking density of the chitin–protein planes and can, therefore, be regarded as a homophase interface.

5. Conclusions

This study was concerned with the experimental observation of structural and mechanical gradients through the thickness of the cuticle of American lobster as a representative example of a hierarchically structured mineralized biological tissue. We found that the exocuticle has a very dense twisted plywood structure and a high stiffness in the range of 8.5–9.5 GPa. The endocuticle showed a much coarser twisted plywood structure and a small stiffness of 3–4.5 GPa. The course of the hardness showed a strong and abrupt change across the interface between the exocuticle and the endocuticle. Within the exocuticle it revealed a gradual increase from about 130 MPa at 100 μm depth to 270 MPa at 300 μm depth. After a small drop from 270 to 240 MPa at 350 μm depth, close to the interface layer between exocuticle and endocuticle, the hardness decreases to a much smaller level between 30 and 55 MPa in the endocuticle. The mechanics observed were qualitatively interpreted in terms of gradients in the honeycomb mechanics of the chitin–protein network.

Acknowledgements

The authors gratefully acknowledge the financial support from the Gottfried–Wilhelm–Leibniz program of the Deutsche Forschungsgemeinschaft (German Research Foundation).

References

[1] Hadley NF. The arthropod cuticle. Sci Am 1986;255:98–106.
[2] Vincent JFV. Structural biomaterials. Princeton (NJ): Princeton University Press; 1990.
[3] Vincent JFV, Wegst UGK. Design and mechanical properties of insect cuticle. Arthropod Struct Dev 2004;33:187–99.
[4] Vincent JFV. Arthropod cuticle: a natural composite shell system. Composites: Part A 2002;33:1311–5.
[5] Vincent JFV, Currey JD, editors. Mechanical properties of biological materials. Cambridge: Society for Experimental Biology; 1980.
[6] Weiner S, Addadi L. Design strategies in mineralized biological materials. J Mater Chem 1997;7:689.
[7] Carlström D. The crystal structure of a-chitin. J Biophys Biochem Cytol 1957;3:669.
[8] Andersen SO. Biochemistry of insect cuticle. Ann Rev Entomol 1979;24:29–61.
[9] Blackwell J, Weih MA. Structure of chitin–protein complexes: ovipositor of the ichneumon fly, *Megagrhyssa*. J Mol Biol 1980;137:49–60.
[10] Lowenstam HA. Minerals formed in organisms. Science 1981;211:1126.
[11] Mann S, Webb J, Williams RJP. On biomineralization. New York (NY): VCH Press; 1989.
[12] Lowenstam HA, Weiner S, editors. On biomineralization. New York (NY): Oxford University Press; 1989.
[13] Mann S. Biomineralization and biomimetic materials chemistry. J Mater Chem 1995;5:935.
[14] Manoli F, Koutsopoulos S, Dalas E. Crystallization of calcite on chitin. J Cryst Growth 1997;182:116.
[15] Falini G, Albech S, Weiner S, Addadi L. Control of aragonite or calcite polymorphism by mollusk shell macromolecules. Science 1996;271:67.
[16] Epple M. Biomaterialien und biomineralisation. Germany: Teubner Verlag; 2003 [in German].
[17] Bouligand Y. Twisted fibrous arrangement in biological materials and cholesteric mesophases. Tissue Cell 1972;4:189.
[18] Giraud-Guille MM. Chitin crystals in arthropod cuticles revealed by diffraction contrast transmission electron microscopy. J Struct Biol 1990;103:232.
[19] Giraud-Guille MM. Fine structure of the chitin–protein system in the crab cuticle. Tissue Cell 1984;16:75.
[20] Giraud-Guille MM. Plywood structures in nature. Curr Opin Solid State Mater Sci 1998;3:221.
[21] Vernberg FJ, Vernberg WB. The biology of crustacea. New York: Academic Press; 1983.
[22] Horst MN, Freeman JA, editors. The crustacean integument. Morphology and biochemistry. Ann Arbor (MI): CRC Press; 1993.
[23] Weiner S, Arad T, Traub W. Crystal organization in rat bone lamellae. FEBS Lett 1991;285:49–54.
[24] Weiner S, Arad T, Sabanay I, Traub W. Rotated plywood structure of primary lamellar bone in the rat: orientations of the collagen fibril arrays. Bone 1997;20:509–14.
[25] Weiner S, Wagner HD. The material bone: structure–mechanical function relations. Annu Rev Mater Sci 1998;28:271–98.
[26] Raabe D, Al-Sawalmih A, Romano P, Sachs C, Brokmeier HG, Yi SB, et al. Structure and crystallographic texture of crustacean bio-composites. In: Proc 14th Int Conf Textures of Materials ICOTOM 14, 2005, Leuven, Belgium, Materials Science Forum. in press.

[27] Gibson LJ, Ashby MF. Cellular solids – structure and properties. 2nd ed. Cambridge: Cambridge University Press; 1997.
[28] Gibson LJ. Biomechanics of cellular solids. J Biomech 2005;38:377–99.
[29] Ashby MF, Gibson LJ, Wegst UFG, Olive R. The mechanical properties of natural materials. I: Material property charts. Proc Roy Soc Lond A 1995;450:123–40.
[30] Gibson LJ, Ashby MF, Karam GN, Wegst UGK, Shercliff HR. The mechanical properties of natural materials. II: Microstructures for mechanical efficiency. Proc Roy Soc Lond A 1995;450:141–62.
[31] Wegst UGK, Ashby MF. The mechanical efficiency of natural materials. Philos Mag 2004;84:2167–81.
[32] Nishino T, Matsui R, Nakamae K. Elastic modulus of the crystalline regions of chitin and chitosan. J Polym Sci B: Polym Phys 1999;37:1191–6.
[33] Ker RF. Some structural and mechanical properties of locust and beetle cuticle. DPhil Thesis, University of Oxford, 1977.
[34] Yamaguchi I, Itoh S, Suzuki M, Sakane M, Osaka A, Tanaka J. The chitosan prepared from crab tendon I: the characterization and the mechanical properties. Biomaterials 2003;24:2031–6.
[35] Xu W, Mulhern PJ, Blackford BL, Jericho MH, Templeton I. A new force microscopy technique for the measurement of the elastic properties of biological materials. Scanning Microscopy 1994;8:499–506.
[36] Vincent JFV. Biomechanics: life among the formulae of physics. Science 2004;304:520.
[37] Vincent JFV. Morphology and design of the extensible intersegmental membrane of the female migratory locust. Tissue Cell 1981;13:831–53.
[38] Currey JD. The failure of exoskeletons and endoskeletons. J Morphol 1967;123:1–16.
[39] Currey JD. Biocomposites: micromechanics of biological hard tissue. Curr Opin Solid State Mater Sci 1996;1:440–5.
[40] Hepburn HR, Joffe I, Green N, Nelson KJ. Mechanical properties of a crab shell. Comp Biochem Physiol 1975;50A:551–4.
[41] Melnick CA, Chen S, Mecholsky JJ. Hardness and toughness of exoskeleton material in the stone crab, *Menippe mercenaria*. J Mater Res 1996;11:2903–7.
[42] Weiner S, Traub W, Wagner HD. Lamellar bone: structure–function relations. J Struct Biol 1999;126:241–55.
[43] Reynolds SE. The mechanical properties of the abdominal cuticle of Rhodnius larvae. J Exp Biol 1975;62:69–80.
[44] Pryor MGM. On the hardening of the ootheca of *Blatta orientalis*. Proc Roy Soc Lond, Ser B 1940;128:378–98.
[45] Jäger IL, Fratzl P. Mineralized collagen fibrils – a mechanical model with a staggered arrangement of mineral particles. Biophys J 2000;79:1737–46.
[46] Gao H, Ji B, Jaeger IL, Arzt E, Fratzl P. Materials become insensitive to flaws at nanoscale: lessons from nature. Proc Nat Acad Sci, USA 2003;100:5597–600.
[47] Fratzl P, Gupta HS, Paschalis EP, Roschger P. Structure and mechanical quality of the collagen–mineral nano-composite in bone. J Mater Chem 2004;14:2115–23.
[48] Fratzl P, Burgert I, Gupta HS. On the role of interface polymers for the mechanics of natural polymeric composites. Phys Chem Chem Phys 2004;6:5575–9.
[49] Fraenkel G, Rudall KM. A study of the physical and chemical properties of insect cuticle. Proc Roy Soc Lond, Ser B 1940;129:1–35.
[50] Andersen SO. The stabilization of locust cuticle. J Insect Physiol 1981;27:393–6.
[51] Vincent JFV, Hillerton JE. The tanning of insect cuticle – a critical review and a revised mechanism. J Insect Physiol 1979;25:653–8.
[52] Vincent JFV, Ablett S. Hydration and tanning in insect cuticle. J Insect Physiol 1988;33:973–9.
[53] Raabe D, Romano P, Al-Sawalmih A, Sachs C, Brokmeier HG, Yi SB, et al. Discovery of a honeycomb structure in the twisted plywood patterns of fibrous biological nano-composite tissue. J Cryst Growth 2005;in press.